In silico design of novel 2H-chromen-2-one derivatives as potent and selective MAO-B inhibitors

ARTICLE *in* EUROPEAN JOURNAL OF MEDICINAL CHEMISTRY · JANUARY 2015

Impact Factor: 3.45 · DOI: 10.1016/j.ejmech.2014.10.029

9 AUTHORS, INCLUDING:

Orazio Nicolotti
Università degli Studi di Bari Aldo Moro
78 PUBLICATIONS **927** CITATIONS
SEE PROFILE

Marco Catto
Università degli Studi di Bari Aldo Moro
49 PUBLICATIONS **1,097** CITATIONS
SEE PROFILE

Estefanía Méndez-Álvarez
University of Santiago de Compostela
50 PUBLICATIONS **1,214** CITATIONS
SEE PROFILE

Angelo Carotti
Università degli Studi di Bari Aldo Moro
225 PUBLICATIONS **4,121** CITATIONS
SEE PROFILE

European Journal of Medicinal Chemistry 89 (2015) 98–105

Contents lists available at ScienceDirect

European Journal of Medicinal Chemistry

journal homepage: http://www.elsevier.com/locate/ejmech

Original article

In silico design of novel 2*H*-chromen-2-one derivatives as potent and selective MAO-B inhibitors

Leonardo Pisani [a], Roberta Farina [a], Orazio Nicolotti [a], Domenico Gadaleta [a], Ramon Soto-Otero [b], Marco Catto [a], Mario Di Braccio [c], Estefania Mendez-Alvarez [b], Angelo Carotti [a, *]

[a] *Dipartimento di Farmacia – Scienze del Farmaco, Università degli Studi di Bari "Aldo Moro", Via E. Orabona, 4, I-70125 Bari, Italy*
[b] *Grupo de Neuroquimica, Departamento de Bioquimica y Biologia Molecular, Facultad de Medicina, Universidad de Santiago de Compostela, San Francisco I, E-15782 Santiago de Compostela, Spain*
[c] *Dipartimento di Scienze Farmaceutiche, Università degli Studi di Genova, Viale Benedetto XV, 3, I-16132 Genova, Italy*

ARTICLE INFO

Article history:
Received 15 May 2014
Received in revised form
7 October 2014
Accepted 12 October 2014
Available online 13 October 2014

Keywords:
Monoamine oxidase inhibitors
4-Substituted-7-(halo)benzyloxy-2*H*-chromene-2-ones
Molecular docking
Selective MAO-B inhibitors
Parkinson's disease
3D-QSAR

ABSTRACT

Inhibition data on rat monoamine oxidase B isoform of a large number of 7-*meta*halobenzyloxy-2*H*-chromen-2-one derivatives (67 compounds) carrying at position 4 a variety of substituents differing in steric, electrostatic, lipophilic and H-bonding properties, were modeled by Gaussian field-based 3D-QSAR and docking simulations carried out on rat MAO-B homology model. The computational study combining two different approaches provided easily interpretable binding modes, highlighting the dominant role of the steric effects at position 4, and guided the design of new, potent and selective MAO-B inhibitors. The 4-hydroxyethyl-, 4-chloroethyl-, 4-carboxamidoethyl-coumarin derivatives **70**, **71**, and **76**, respectively, were endowed with high MAO-B inhibitory potency (pIC_{50} = 8.13, 7.89 and 7.82, respectively) and good selectivity over MAO-A (pIC_{50} = 5.33, 3% inhibition at 10 μM, and pIC_{50} = 5.37, respectively). New compounds with moderate to low MAO-B inhibitory activity were also designed and prepared to challenge the predictive power of our docking-based 3D-QSAR model. The good match between predicted and experimental pIC_{50} values for all the newly designed compounds confirmed the robustness of our model (r^2 = 0.856, RMSE = 0.421) and its transparent rationale in unveiling the main molecular determinants for high potency towards MAO-B.

1. Introduction

Monoamine oxidases (MAOs, EC 1.4.3.4) are flavoenzymes that catalyze the Cα-H oxidation of unhindered arylalkylamines [1] The MAO-driven oxidative deamination leads to the inactivation of many exogenous as well as endogenous aminic substrates, including dietary components (e.g., tyramine) and neurotransmitters (e.g., serotonin, histamine and catecholamines), and to the bioactivation of the Parkinson-inducing neurotoxin 1-methyl-4-phenyl-1,2,3,6-tetrahydropyridine (MPTP). The two known and fully characterized enzymatic isoforms of MAO, named MAO-A and MAO–B [2], share 70% sequence identity [3] but differ for substrates and inhibitors sensitivity, tissue distribution [4] and three-dimensional structural motifs [5–7]. In the catecholaminergic system the prevalent isoform is MAO-A, whereas MAO-B predominates in cerebral districts under serotonin regulation. MAO-A degrades preferentially serotonin and is selectively inhibited by clorgyline. On the other side, MAO–B isoform is blocked by selegiline and deaminates preferentially 2-phenylethylamine. Both isoenzymes are able to catabolize catecholamines with similar rates [8].

Since MAOs play a major role in controlling the levels of several neurotransmitters, mainly in the CNS, their therapeutic potential has been clearly related to the treatment of neuropathies [9]. The earliest inhibitors developed as antidepressant (e.g., tranylcypromine) showed no isoform selectivity and an irreversible mechanism (suicide-type inhibitors). Therefore, many of them have been discontinued because of severe side effects (i.e., hepatotoxicity and hypertensive crisis) and tedious dietary restrictions. Propargylamine-bearing derivatives clorgyline, a selective MAO-A inhibitor, and selegiline and rasagiline, two selective MAO-B inhibitors, showed improved safety because of their enhanced

* Corresponding author.
E-mail addresses: carotti_angelo@hotmail.com, angelo.carotti@uniba.it (A. Carotti).

http://dx.doi.org/10.1016/j.ejmech.2014.10.029
0223-5234/

Table 1
Chemical structure and MAO inhibition data of coumarin training and test set for 3D-QSAR Model.

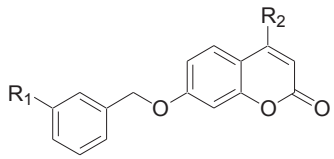

Compd	R_1	R_2	Observed MAO-B inhibitory activity[a]	Predicted MAO-B inhibitory activity[b]
1	Cl	H	7.77	7.40
2	Cl	Me	8.13	7.44
3	Cl	Et	7.54	7.45
4	Cl	CF_3	6.06	6.93
5	Cl	Cl	7.68	7.05
6	Cl	CH_2Cl	7.36	7.33
7	Br	CH_2Cl	6.68	7.47
8	H	OH	5.04	5.21
9	F	OH	5.68	5.42
10	Cl	OH	6.32	5.77
11	Br	OH	6.31	5.87
12	Cl	NH_2	7.32	7.50
13	Cl	CHO	7.28	7.64
14	Cl	$COCH_3$	7.40	7.40
15	Cl	COOH	4.00[c]	4.49
16	Cl	COOEt	6.38	6.35
17	Cl	$CONH_2$	6.63	6.60
18	Cl	CN	6.99	7.04
19	Cl	CH=NOH	6.66	6.92
20	Cl	CH_2OH	8.28	8.11
21	Br	CH_2OH	7.85	8.22
22	Cl	$CH(OH)CH_3$	7.11	7.38
23	Cl	CH_2CN	7.80	7.78
24	Cl	CH_2CONH_2	7.52	8.09
25	Cl	$CH_2CONHMe$	7.62	7.79
26	Cl	$CH_2CON(Me)_2$	7.40	7.85
27	Cl	CH_2NH_2	7.82	7.66
28	Cl	CH_2NHMe	7.89	7.70
29	Br	CH_2NHMe	7.96	7.53
30	Cl	CH_2NHnPr	6.69	6.94
31	Cl	CH_2NHnBu	6.35	6.70
32	Cl	$CH_2N(Me)_2$	5.95	6.96
33	Cl	CH_2-1′-pyrrolidinyl	5.77	6.06
34	Cl	CH_2-4′-morpholinyl	5.64	5.81
35	H	OMe	7.00	6.91
36	F	OMe	7.44	7.15
37	Cl	OMe	8.11	7.46
38	Br	OMe	8.24	7.55
39	H	OEt	6.12	6.59
40	F	OEt	6.58	6.82
41	Cl	OEt	6.94	6.86
42	Br	OEt	6.90	7.29
43	H	OnPr	6.24	6.05
44	F	OnPr	6.39	6.26
45	Cl	OnPr	7.21	6.92
46	Br	OnPr	7.13	7.08
47	Cl	OiPr	4.61	5.61
48	Cl	OCH_2OMe	7.00	7.16
49	Cl	OCH_2SMe	6.50	7.09
50	Cl	OCH_2CN	7.34	7.45
51	Cl	OPh	5.39	5.33
52	Cl	NHMe	8.06	7.37
53	Cl	NHEt	7.55	6.70
54	Cl	NHiPr	5.11	5.75
55	Cl	NHPh	5.01	5.37
56	Cl	$NHCOCH_3$	7.41	7.08
57	Cl	NHCOOEt	6.23	5.62
58	Cl	NHCONHEt	4.50[c]	4.85
59	Cl	OCH_2COCH_3	7.57	7.44
60	Cl	OCH_2COOH	4.50[c]	4.79
61	Cl	OCH_2COOEt	5.74	6.08
62	Cl	OCH_2CONH_2	8.48	8.44
63	Br	OCH_2CONH_2	8.05	8.53
64	Cl	$OCH_2CONHMe$	7.47	7.07
65	Cl	$OCH_2CON(Me)_2$	6.30	5.80
66	Cl	OCH_2CO-1′-piperidinyl	4.41	3.98
67	Cl	OCH_2CO-4′-morpholinyl	4.89	4.84

[a] MAO-B inhibitory activities are expressed as pIC_{50} (*M*). Values are the mean of two or three independent experiments. SEM of the IC_{50} values were within ±10%.
[b] pIC_{50} values predicted by our Gaussian-based 3D-QSAR model with Phase.
[c] Estimated value from the % of inhibition at 10 μM concentration.

isoform selectivity and are currently used as antidepressant and as dopamine-sparing agents against Parkinson's disease (PD), respectively [10–12].

In addition to these well-consolidated pharmacological actions, MAO inhibitors have recently been exploited as potential therapeutics to combat severe age-related neurodegenerative diseases (NDs) [13], such as Alzheimer's disease (AD), amyotrophic lateral sclerosis (ALS) and Huntington's disease (HD). Several biochemical abnormalities in neurons underlie these debilitating syndromes, spanning from protein misfolding to bio-metal dyshomeostasis and including mitochondrial impairment and oxidative stress. The catalytic cycle of MAOs produces as one of the end-products hydrogen peroxide, which is a precursor of harmful reactive oxygen species (ROS) and a toxic oxidant itself. When the physiological radical detoxification system is altered as it is in NDs, MAOs become a source of oxidative stress and their inhibition may result in a neuroprotective activity [14,15]. Moreover, the analysis of post-mortem AD patients brain tissues pointed out an increased MAO-B expression in plaques-related astrocytes [16].

For these reasons, we have performed a series of studies on the design, synthesis and biological evaluation of selective MAO inhibitors [17], and on dual acetylcholinesterase and MAO-B inhibitors as well [18], looking for potential therapeutics for NDs [19]. Within this frame we have reported the discovery of novel selective MAO B inhibitors with favorable physicochemical and pharmacokinetic profiles carrying properly selected substituents at position 4 of 7-benzyloxy-substituted coumarins [20]. More recently, a large number of new coumarin derivatives were synthesized through a fine molecular tuning at position 4 aimed at an optimization of the MAO affinity and selectivity profiles [21]. The inhibitory activity towards MAO-B together with the MAO-B over MAO-A selectivity have been carefully evaluated, but only in qualitative terms. To gain more significant insights into the pivotal physicochemical interactions governing MAO inhibition, we therefore modeled the inhibition data for a large panel of sixtyseven coumarin derivatives through Gaussian field-based 3D-QSAR method and docking simulations. These compounds carry a (3′-halo)benzyloxy group as the common substituent at position 7 and differ for the substituents placed at position 4 of the coumarin skeleton. The modeling studies provided easily interpretable binding modes and guided the design of new, potent and selective inhibitors by exploiting our expertise on coumarin-based MAO inhibitors [22,23]. New compounds with moderate or low MAO-B inhibitory activity were also designed and prepared in order to challenge the predictive power of our model. We obtained good predictions for all the newly prepared compounds, thus demonstrating the solid statistics of our model as well as its real-life potential for optimizing potency towards MAO-B. The novel molecules here reported may be considered promising hit compounds for the discovery of new neuroprotectants and for the development of multi-target directed ligands having MAO-B inhibition as the core activity.

2. Computational studies: development of a Gaussian-field based 3D-QSAR model

The inhibition data (Table 1) of a series of 67 MAO inhibitors recently published by us [21] were subjected to a 3D-QSAR study to extend and complement the results of the docking screen aiming at finding at a 3D level a causative correlation among the variation of the biological affinity and relevant molecular properties. The initial pool of 67 compounds was split into a training set and a test set, containing 58 and 9 molecules, respectively, having a similar coverage in terms of biological activity range and structural diversity. The test set is composed of about 15% of the whole set of molecules. This set exhibited good spread and distribution of the biological activity values and represented the structural diversity of the examined molecules.

The 3D-QSAR study was complemented by docking simulations [21] of all the molecules in the training and test set onto rat MAO-B by means of GOLD 5.2 program [24]. The interested reader is referred elsewhere for additional experimental details [20,21,23]. The molecular overlay for the derivation of the 3D-QSAR model was obtained by superimposing top-scored poses resulting from docking simulations. A very limited manual intervention was carried out to maximize, when necessary, the structural match of the 7-substituted coumarin common scaffold and minimize the occurrence of spurious signals due to structural noise rather than to variance of the sampled molecular properties [25]. By using the Gaussian-based fields available [26] in Phase (included in the Schroedinger suite) [27], the inhibitory potency towards MAO-B was related via Partial Least Squares (PLS) to the variation of the steric, electrostatic, hydrophobic, hydrogen bond donor (HBD) and hydrogen bond acceptor (HBA) fields using a grid space equal to 1.0 Å. As shown in Fig. 1a, the obtained 3D-QSAR model disclosed solid statistics for both the training (n = 58, r^2 = 0.856, RMSE = 0.421, stability = 0.853, factors = 4, q^2 = 0.605) and test (n = 9, r^2_{ext} = 0.794, RMSE = 0.457) set.

A fine and robust statistical and chemical interpretability is an important aspect of 3D-QSAR models and to this end a careful analysis of statistical parameters of the developed model was performed. The higher contribution to the model was ensured by the steric field (32.10%) and, then, in decreasing order, by the hydrophobic (25.80%), the electrostatic (23.30%), the HBD (12.60%) and HBA (6.20%) fields. Satisfactorily, the relative weight of any field in the 3D-QSAR model in determining sound explanations on

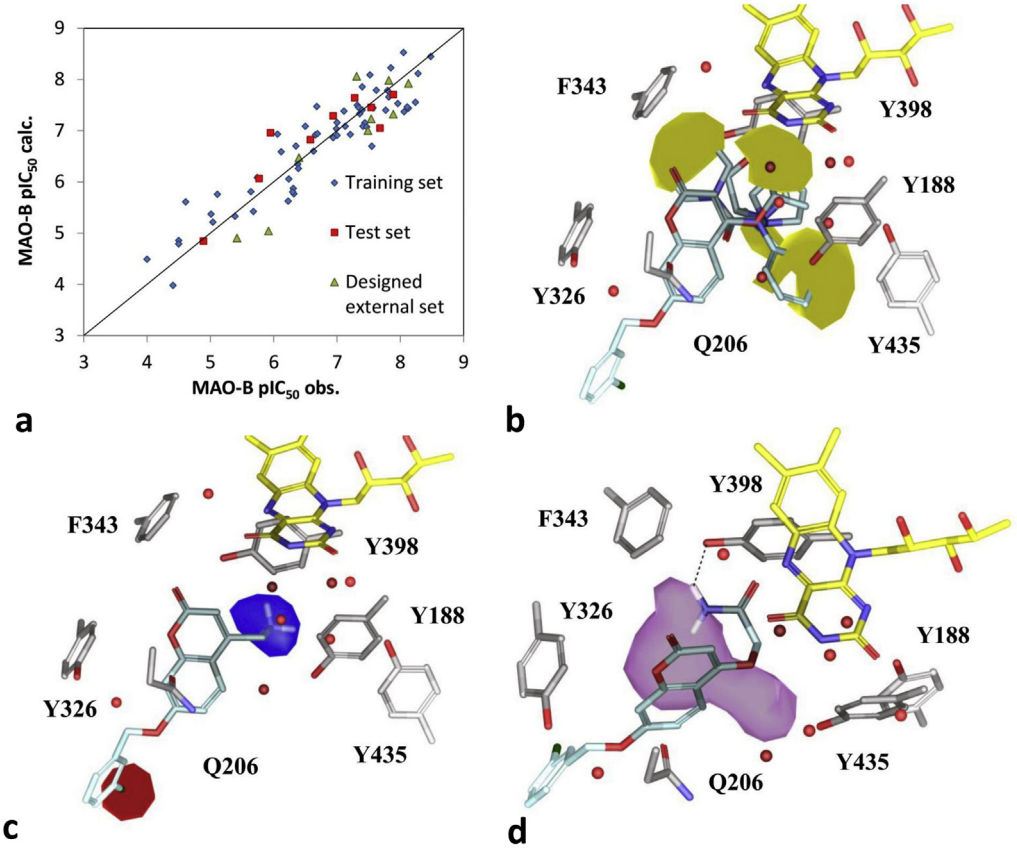

Fig. 1. Graphical plot of observed and calculated pIC_{50} values (1a) and 3D-QSAR isocontour maps (1b–d). (1a) Comparison between the observed and calculated pIC_{50} values for MAO-B inhibition. Molecules of the training, test and experimental external sets (see text below) are represented as blue diamonds, red squares and green triangles, respectively. (1b) Gaussian field-based 3D-QSAR steric isocontour maps. FAD is shown in yellow while the eight structured water molecules as red spheres. Nitrogen and oxygen atoms are in blue and red, respectively. The aminoacid side chains are indicated in gray and the inhibitor molecules in cyan. Contour levels are set to $-7.5\ 10^{-3}$ StdDev*Coeff (yellow). Inhibitors **33** (pIC_{50} = 5.77), **34** (pIC_{50} = 5.64), **47** (pIC_{50} = 4.61), **51** (pIC_{50} = 5.39), **55** (pIC_{50} = 5.01), and **66** (pIC_{50} = 4.41) along with a number of amino acid side chains from the rat MAO-B binding sites are shown to help interpretation. (1c) Gaussian field-based 3D-QSAR electrostatic isocontour maps. FAD is shown in yellow while the eight structured water molecules as red spheres. Nitrogen and oxygen atoms are in blue and red, respectively. The aminoacid side chains are indicated in gray and the inhibitor molecules in cyan. Contour levels are set to $1.5\ 10^{-2}$ StdDev*Coeff (blue) and $-4.0\ 10^{-4}$ StdDev*Coeff (red). Inhibitor **27** (pIC_{50} = 7.82) along with a number of amino acid side chains from the rat MAO-B binding sites are shown to help interpretation. (1d) Gaussian field-based 3D-QSAR HBD isocontour maps. FAD is shown in yellow while the eight structured water molecules as red spheres. Nitrogen and oxygen atoms are in blue and red, respectively. The aminoacid side chains are indicated in gray and the inhibitor molecules in cyan. Contour levels are set to $2.0\ 10^{-3}$ StdDev*Coeff (violet). Inhibitor **62** (pIC_{50} = 8.48) along with a number of amino acid side chains from the rat MAO-B binding sites are shown to help interpretation. The black dashed line indicates the HB established by the ligand with Y398. (For interpretation of the references to colour in this figure legend, the reader is referred to the web version of this article.)

Table 2
Chemical structure and MAO inhibition data of coumarin derivatives **70**–**73** and **75**–**79**.

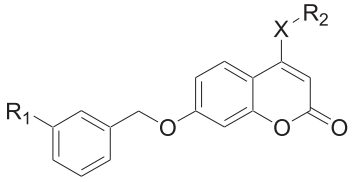

Compd	R_1	X	R_2	Observed MAO-A inhibitory activity[a]	Observed MAO-B inhibitory activity[a]	Predicted MAO-B inhibitory activity[b]
70	Cl	CH_2	CH_2OH	5.33	8.13	7.92
71	Cl	CH_2	CH_2Cl	3 ± 0.2%	7.89	7.32
72	Cl	CH_2	CH_2Br	22 ± 1.7%	7.49	7.00
73	Cl	CH_2	CH_2-piperidin-1-yl	1 ± 0.2%	5.42	4.90
75	Cl	CH_2	CH_2COOH	13 ± 0.5%	5.92	5.04
76	Cl	CH_2	CH_2CONH_2	5.37	7.82	7.98
77	Cl	CH_2	CH_2CN	22 ± 1.3%	7.54	7.23
78	Cl	NH	CH_2CONH_2	7.02	7.31	8.06
79	Cl	NH	$COCH_2Cl$	5.24	6.40	6.47

[a] MAO-A and MAO-B inhibitory activities are expressed as pIC_{50} (*M*) or as percentage of inhibition at 10 μM. Values are the mean of two or three independent experiments.
[b] pIC_{50} values predicted by our Gaussian-based 3D-QSAR model with phase.

the nature of the molecular interactions governing the binding towards MAO-B was in agreement with our preliminary SAR analyses [21] highlighting the highest relevance of steric effects at position 4. For the ease of representation, meaningful examples showing how the variation of the Gaussian based molecular fields was related to that of the MAO-B inhibitory activity were reported in Fig. 1b–d.

As shown in Fig. 1b, the existence of a larger forbidden steric region, plastically contoured by yellow polyhedra, was sustained by a number of bulky groups, bound to position 4, playing a detrimental effect for MAO-B inhibitory activity. More specifically, such substituents were the piperidinyl (**66**, pIC_{50} = 4.41), phenyl (**55**, pIC_{50} = 5.01; **51**, pIC_{50} = 5.39), morpholinyl (**34**, pIC_{50} = 5.64), pyrrolidinyl (**33**, pIC_{50} = 5.77) and isopropyl (**54**, pIC_{50} = 5.11) moieties whose steric effects were clearly unfavorable to MAO-B inhibitory potency. On Fig. 1c, blue areas (in web version) contoured regions accommodating positively charged substituents, as those of protonated amines (e.g., **27**, pIC_{50} = 7.82), increased MAO-B activity while red areas captured the positive effect on MAO-B activity of the electron-rich and large bromine and chlorine substituents at the position *meta* of the 7-benzyloxy substituent [28]. Finally on Fig. 1d, the violet polyhedra indicated the occurrence of HBD interactions favoring MAO-B inhibition. In fact, the most active derivative provided with HBD groups (**62**, pIC_{50} = 8.48) impacted this area. In particular, it was observed by docking simulations that compound **62** was engaged in HB interactions with the hydroxyl of Y398 at the MAO-B binding site.

The field-based 3D-QSAR model was then employed for the computer-assisted design of new biologically active coumarin-based MAO-B inhibitors (Table 2). The overarching aim was that of improving or at least maintaining a high inhibitory activity while keeping the overall molecular lipophilicity at an acceptable level. To this aim, selected substituents at position 4 were introduced. Most of them carried unhindered hydrophilic groups exhibiting HB donor/acceptor properties (hydroxyl, carboxamido and cyano groups). Importantly, the occurrence of HB interactions was welcomed to optimize MAO-B inhibition.

3. Chemistry

Besides the already described compounds (Table 1), a new series of MAO inhibitors has been designed and prepared by following the synthetic pathways illustrated in Schemes 1–3.

As depicted in Scheme 1, the preparation of compounds **70**–**73** started from the LiOH-mediated hydrolysis of ethyl ester **68** [20]. The carboxylic acid functionality of compound **69** underwent a regioselective reduction to the corresponding primary alcohol yielding derivative **70** by using borane·dimethylsulfide complex that maintained the lactone moiety unaffected. Chlorination of this alcohol in a refluxing benzene/thionyl chloride mixture afforded coumarin **71**. The starting alcohol **70** was transformed into the corresponding bromide **72** in the presence of carbon tetrabromide and triphenylphosphine in anhydrous dichloromethane. Nucleophilic displacement of primary bromide with an excess of piperidine furnished compound **73**. The synthetic pathway leading to amide **76** (Scheme 2) required the alkylation of the enolate of diethyl malonate with the substituted chloromethylcoumarin **6**

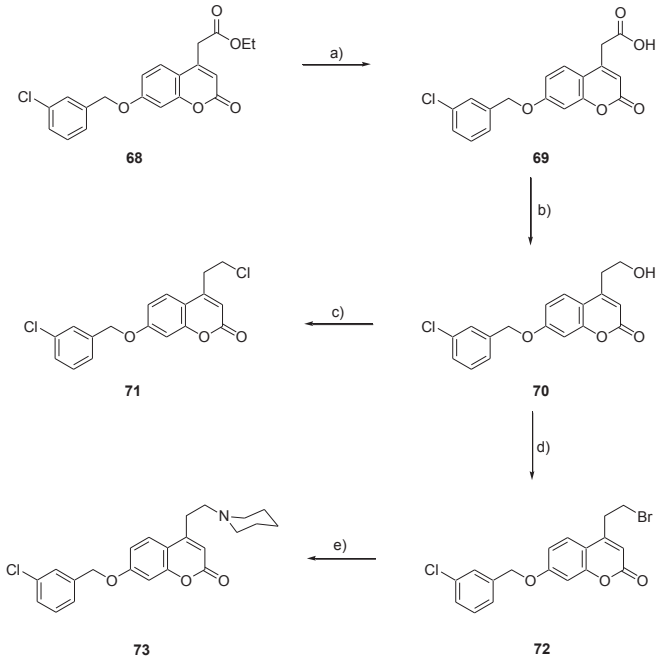

Scheme 1. Synthesis of coumarin derivatives **70**–**73**. Reagents and conditions: a) LiOH·H_2O, THF/H_2O (3/1, v/v), room temperature, 15 h; b) borane· dimethyl sulfide complex, dry THF, −15 °C to room temperature, 4 h; c) thionyl chloride, benzene, reflux, 12 h; d) carbon tetrabromide, triphenylphosphine, dry dichloromethane, room temperature, 3 h; e) piperidine, dry THF, room temperature, 15 h.

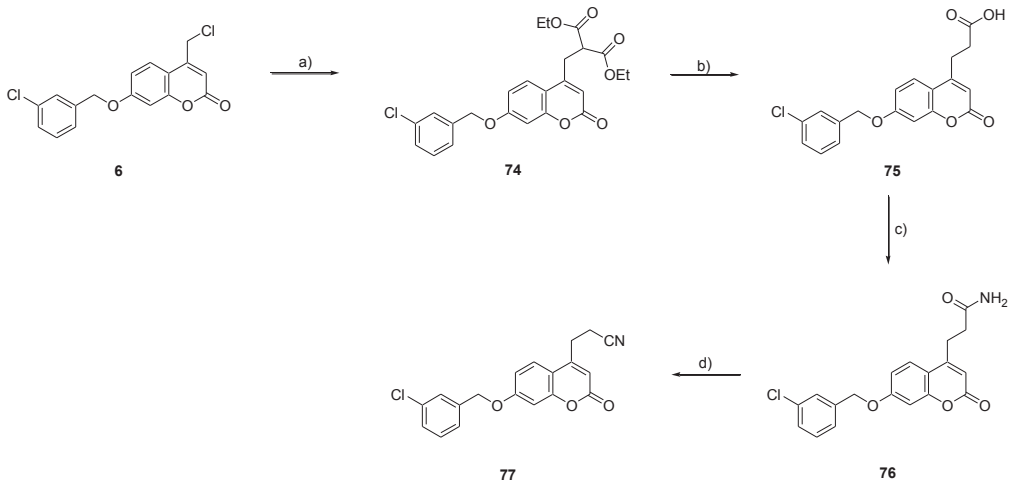

Scheme 2. Synthesis of coumarin derivatives **75**–**77**. Reagents and conditions: a) diethyl malonate, NaH, DMSO, room temperature, 30 min; b) i: NaOH, abs. ethanol, reflux, 2 h; ii: DMSO, reflux, 1 h; c) i: thionyl chloride, dry dichloromethane, reflux, 2 h; ii: aq. NH_3, 0 °C to room temperature, 15 h; d) trifluoroacetic anhydride, pyridine, dry dioxane, room temperature, 1 h.

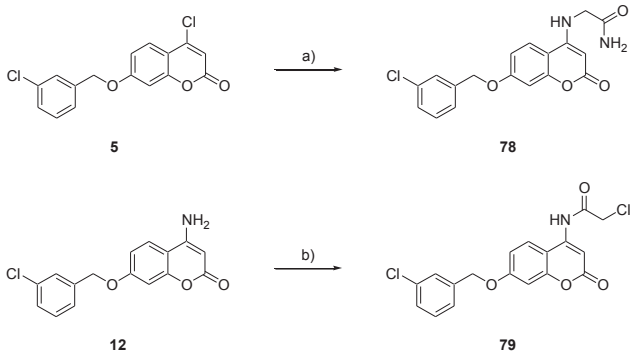

Scheme 3. Synthesis of coumarin derivatives **78**–**79**. Reagents and conditions: a) $GlyNH_2 \cdot HCl$, DIEA, dry DMF, 90 °C, 4 h; b) chloroacetyl chloride, DIEA, dry THF, reflux, 48 h.

[29]. After saponification of mono-substituted diethyl malonate **74** with sodium hydroxide in refluxing ethanol, the resulting malonic acid was submitted to a thermal decarboxylation that allowed to obtain **75**. The carboxylic acid was activated as acyl chloride before reacting with ammonia to obtain primary amide **76**. The dehydration of the amidic functionality to nitrile was accomplished with trifluoroacetic anhydride and pyridine in dioxane [30], thus obtaining compound **77**. Derivatives **78** and **79**, bearing a more rigid lateral chain at position 4, were obtained through substitution of the appropriate 4-chlorocoumarin **5** [21] with glycinamide and acylation of suitable 4-aminocoumarin **12** [21] with chloroacetyl chloride, respectively (Scheme 3).

4. Biological assays

The inhibition of monoamine oxidases A and B activity (Tables 1 and 2) was measured *in vitro* by using crude rat brain mitochondrial homogenates through a spectrophotometric method [31] based on the monitoring of the oxidation rate of the non-selective non-fluorescent MAO substrate kynuramine to 4-hydroxyquinoline. The percentage of MAO inhibition was determined for all the examined compounds at 10 μM concentration and IC_{50} data were measured only for compounds showing an inhibition greater than 50%. In a few cases the IC_{50} was measured also for compounds with low activity (MAO-I < 50% at 10 μM) when deemed necessary for a quantitative evaluation of the structure-activity and/or structure–selectivity relationships (SAR and SSR, respectively). Inhibitory potencies, expressed as pIC_{50} or % of MAO inhibition, are reported in Tables 1 and 2 along with the chemical structures of the examined 4,7-disubstituted coumarins. To avoid the loss of important structural information in the derivation of sound SAR, for the low active acid (**15** and **60**, Table 1) and ureido (entry **58**, Table 1) MAO-B inhibitors, estimated pIC_{50} values of 4.0 and 4.5 were used.

5. Assessing the predictive power of the 3D-QSAR model: results and discussion

At a first glance, the inhibition data reported in Tables 1 and 2 indicated that most of the examined coumarin derivatives exhibited a very high and selective inhibition of MAO B.

Among the newly designed compounds, coumarins derivatives **70**, **76** (and its isoster **78**) and **77** showed indeed nanomolar MAO-B affinities ($7.31 < pIC_{50} < 8.13$).

To detect further molecular determinants influencing binding interactions, lipophilic groups were also introduced in the branching chain at position 4. As predicted by 3D-QSAR model, the additional lipophilic interactions allowed by chlorine (**71**, $pIC_{50} = 7.89$) and bromine (**72**, $pIC_{50} = 7.49$) led to potent MAO-B inhibitors, being the affinity controlled also by the different steric hindrance.

Moreover, two weakly active inhibitors were also designed and tested to further challenge the predictive capability of the field-based 3D-QSAR model and to prove its real-life potential for the design of MAO-B selective inhibitors. As expected and predicted, the insertion of sterically encumbered (i.e., **73**, $pIC_{50} = 5.42$) or ionizable acid groups (i.e., **75**, $pIC_{50} = 5.92$) resulted in the least active derivatives of this newly designed small series of inhibitors. The carboxylic acid derivative **75** may be considered an outlier and this is not surprising as in the training set the only two acids included have an estimated activity value, as only % of inhibition at 10 μM were available.

The whole series of the newly designed compounds reported in Table 2 was subjected to docking simulations and the best poses therein used for external validation of the field-based 3D-QSAR model [32]. Satisfactorily, predicted and observed values returned a very good match. In particular, the values of external r^2 and the

RMSE were equal to 0.850 and 0.510, respectively (Fig. 1a). The slope of the regression line was equal to 0.735 and the intercept on *y*-axis is equal to 2.046. Even forcing the regression line through origin of axes, statistics were acceptably solid with the value of external r^2 being 0.715.

6. Conclusions

A large set of coumarin derivatives carrying substituents with different stereoelectronic, lipophilic and hydrogen bonding features at position 4 was used to derive a Gaussian field-based 3D-QSAR model able to interpret the structure-inhibitory activity data in quantitative terms at the three-dimensional level. The model showed a good predictive as well as descriptive power and shed light on the main molecular determinants for high affinity towards MAO-B isoform and allowed a fine interpretation of the binding modes of the examined derivatives. In particular, the binding interactions were mainly controlled by the steric hindrance of the substituents at position 4 of the coumarin backbone and also by their lipophilic character and HB properties. By applying this model to the design of novel MAO-B inhibitors, a small focused series of coumarin-based inhibitors was developed. The biological evaluation of these novel 4,7-substituted coumarin derivatives highlighted the robustness of our model and returned several inhibitors with an outstanding MAO-B over MAO-A isoform selectivity and MAO-B inhibitory potencies in the low nanomolar range (compounds **70**, **71**, **72**, **76**, **77** and **78**). The molecules here reported may be considered promising hit compounds with a potential neuroprotective activity and they can be further exploited for the design of multi-target directed ligands showing MAO-inhibition as the central activity.

7. Experimental section

7.1. Chemistry

Starting materials, reagents and analytical grade solvents were purchased from Sigma–Aldrich Europe. The purity of all the intermediates, checked by ^{1}H NMR and HPLC was always better than 95%. All the newly prepared and tested compounds showed an HPLC purity higher than 98%. Column chromatography was performed using Merck silica gel 60 (0.063–0.200 mm, 70–230 mesh). Flash chromatographic separations were performed on Biotage SP1 purification system using flash cartridges prepacked with KP-Sil 32–63 μm, 60 Å silica. All reactions were routinely checked by TLC using Merck Kieselgel 60 F_{254} aluminum plates and visualized by UV light or iodine. Regarding the reaction requiring the use of dry solvents, the glassware was flame-dried and then cooled under a stream of dry argon before the use. Nuclear magnetic resonance spectra were recorded on a Varian Mercury 300 instrument (at 300 MHz) at ambient temperature in the specified deuterated solvent. Chemical shifts (δ) are quoted in parts per million (ppm) and are referenced to the residual solvent peak. The coupling constants *J* are given in Hertz (Hz). The following abbreviations were used: s (singlet), d (doublet), dd (doublet of doublet), t (triplet), q (quadruplet), m (multiplet), br s (broad signal); signals due to OH and NH protons were located by deuterium exchange with D_2O. Elemental analyses were performed on the EuroEA 3000 analyzer only on the final compounds tested as MAOs inhibitors. The measured values for C, H, and N agreed to within ±0.40% of the theoretical values. Melting points were determined by the capillary method on a Stuart Scientific SMP3 electrothermal apparatus and are uncorrected. Synthesis, analytic and spectroscopic data of compounds **1**–**67** [21] and **72** [20] have been already reported in the literature.

7.1.1. Ethyl {7-[(3-chlorobenzyl)oxy]-2-oxo-2H-chromen-4-yl} acetate (**68**)

Ethyl (7-hydroxy-2-oxo-2*H*-chromen-4-yl)acetate (4.0 g, 8.0 mmol) [29] was dissolved in dry THF (60 mL) and then 3-chlorobenzyl alcohol (3.8 mL, 32 mmol) and ADDP (8.0 g, 32 mmol) were added. A solution of triphenylphosphine (8.4 g, 32 mmol) in dry THF (20 mL) was added dropwise while cooling at 0 °C. The reaction mixture was then stirred at room temperature for 24 h. After removal of the solvent under reduced pressure, the oil residue was purified through flash chromatography (gradient eluant: ethyl acetate in *n*-hexane 0%→60%). Yield: 53%. Spectroscopic data are in agreement with those reported in the literature [20].

7.1.2. {7-[(3-Chlorobenzyl)oxy]-2-oxo-2H-chromen-4-yl}acetic acid (**69**)

Intermediate **68** (1.6 g, 4.1 mmol) was dissolved in a THF/water 3/1 (v/v) mixture (18 mL) and then $LiOH\cdot H_2O$ (0.50 g, 12 mmol) was added. The reaction mixture was stirred at room temperature overnight and then THF was evaporated under reduced pressure. The resulting solution was acidified by the slow addition of HCl 1.0 N while cooling at 0 °C. The resulting precipitate was filtered and washed with abundant water, yielding the desired acid in quantitative yield. Yield: 100%. ^{1}H NMR (300 MHz, DMSO-d_6) δ: 3.86 (s, 2H), 5.23 (s, 2H), 6.31 (s, 1H), 7.03–7.08 (m, 2H), 7.37–7.46 (m, 3H), 7.53 (s, 1H), 7.62 (d, J = 8.8 Hz, 1H), 12.80 (s, 1H, dis. with D_2O).

7.1.3. 7-[(3-Chlorobenzyl)oxy]-4-(2-hydroxyethyl)-2H-chromen-2-one (**70**)

Acid **69** (1.4 g, 4.0 mmol) was dissolved in dry THF (14 mL) and borane·dimethylsulfide complex (0.43 mL, 6.0 mmol) was added dropwise while cooling at −15 °C. The reaction was slowly warmed at room temperature and stirred for 4 h. Methanol was carefully added while cooling at 0 °C and then the mixture was stirred for 30 min. After evaporation of the solvent, the residue was diluted with water (150 mL) and extracted with ethyl acetate (3 × 100 mL). The organic phases were collected, dried over Na_2SO_4 and concentrated thus furnishing a residue that was purified through flash chromatography (gradient eluant: methanol in dichloromethane 0%→10%). Yield: 84%. Mp: 108–9 °C. Anal. ($C_{18}H_{15}ClO_4$) C, H. Spectroscopic data are in agreement with those reported in the literature [20].

7.1.4. 7-[(3-Chlorobenzyl)oxy]-4-(2-chloroethyl)-2H-chromen-2-one (**71**)

Alcohol **70** (0.18 g, 0.54 mmol) was dissolved in benzene (2 mL) and thionyl chloride (0.50 mL) was added. The mixture was refluxed for 12 h and then concentrated to dryness. Separation through flash column chromatography (gradient eluant: ethyl acetate in *n*-hexane 30%→60%) yielded the desired product as a yellow solid. Yield: 73%. Mp: 107–8 °C. ^{1}H NMR (300 MHz, DMSO-d_6) δ: 3.26 (t, J = 6.6 Hz, 2H), 3.96 (t, J = 6.6 Hz, 2H), 5.24 (s, 2H), 6.28 (s, 1H), 7.04 (dd, J_1 = 2.2 Hz, J_2 = 8.8 Hz, 1H), 7.09 (d, J = 2.2 Hz, 1H), 7.40–7.44 (m, 3H), 7.54 (s, 1H), 7.78 (d, J = 8.8 Hz, 1H). Anal. ($C_{18}H_{14}Cl_2O_3$) C, H.

7.1.5. 7-[(3-Chlorobenzyl)oxy]-4-(2-piperidin-1-ylethyl)-2H-chromen-2-one hydrochloride (**73**)

Bromo-derivative **72** (0.11 g, 0.28 mmol) was dissolved in dry THF (2.5 mL) followed by the addition of an excess of piperidine (0.20 mL, 1.7 mmol). After stirring at room temperature for 15 h, the mixture was concentrated under reduced pressure and purified through flash chromatography (gradient eluant: ethyl acetate in *n*-hexane 40% → 90%). The resulting free amine was transformed into

the corresponding hydrochloride by treatment with a commercially available solution of HCl 4.0 N in dioxane. Yield: 79%. Mp: 228–230 °C. ^{1}H NMR (300 MHz, DMSO-d_6) δ: 1.39–1.44 (m, 1H), 1.69–1.84 (m, 5H), 2.85–2.95 (m, 2H), 3.28–3.32 (m, 3H), 3.41 (br s, 1H), 3.51–3.54 (m, 2H), 5.25 (s, 2H), 6.27 (s, 1H), 7.07 (dd, J_1 = 2.5 Hz, J_2 = 8.8 Hz, 1H), 7.11 (d, J = 2.5 Hz, 1H), 7.40–7.42 (m, 3H), 7.53 (s, 1H), 7.88 (d, J = 8.8 Hz, 1H), 10.25 (br s, 1H, dis. with D_2O). Anal. ($C_{23}H_{25}Cl_2NO_3$) C, H, N.

7.1.6. Diethyl ({7-[(3-chlorobenzyl)oxy]-2-oxo-2H-chromen-4-yl} methyl)malonate (**74**) [33]

Diethyl malonate (2.0 mL, 13 mmol) was added dropwise to a suspension of NaH (60% wt. dispersion in mineral oil, 0.53 g, 13 mmol) in dry DMSO (12 mL). The mixture was kept under magnetic stirring at room temperature till a clear solution was obtained (30 min). Then chloromethyl-coumarin **6** [29] (2.2 g, 6.5 mmol) was added. The mixture was stirred at room temperature for 30 min and then quenched by the slow addition of HCl 1.0 N (100 mL), while cooling at 0–5 °C. After extraction with ethyl acetate (3 × 80 mL), the organic layers were collected, dried over Na_2SO_4 and concentrated to dryness. The resulting crude oil was purified through flash chromatography (gradient eluant: ethyl acetate in *n*-hexane 0% → 60%). Yield: 69%. ^{1}H NMR (300 MHz, DMSO-d_6) δ: 1.10 (t, J = 7.1 Hz, 6H), 3.26 (d, J = 7.5 Hz, 2H), 3.97 (t, J = 7.5 Hz, 1H), 4.09 (q, J = 7.1 Hz, 4H), 5.23 (s, 2H), 6.15 (s, 1H), 7.03 (dd, J_1 = 2.5 Hz, J_2 = 8.8 Hz, 1H), 7.08 (d, J = 2.5 Hz, 1H), 7.39–7.43 (m, 3H), 7.53 (s, 1H), 7.79 (d, J = 8.8 Hz, 1H).

7.1.7. 3-{7-[(3-Chlorobenzyl)oxy]-2-oxo-2H-chromen-4-yl} propanoic acid (**75**)

The substituted malonate-intermediate **74** (0.80 g, 1.8 mmol) was suspended in abs. ethanol (25 mL) and solid NaOH (0.80 g, 20 mmol) was added. The mixture was refluxed for 2 h, then cooled at room temperature and concentrated to dryness. After acidification through the addition of 50 mL of HCl 2.0 N, the suspension was kept under vigorous stirring at room temperature overnight. The resulting mixture was filtered and the obtained solid (0.65 g, corresponding to the malonic acid intermediate) was dissolved in dry DMSO (6.0 mL) and kept at reflux for 1 h. After cooling at room temperature, crushed ice (~30 g) was added. The solid was filtered and washed with abundant water thus yielding the desired product with high purity. Yield: 83%. Mp: 181–2 °C. ^{1}H NMR (300 MHz, DMSO-d_6) δ: 2.61 (t, J = 7.7 Hz, 2H), 2.99 (t, J = 7.7 Hz, 2H), 5.23 (s, 2H), 6.14 (s, 1H), 7.03 (dd, J_1 = 2.5 Hz, J_2 = 8.8 Hz, 1H), 7.07 (d, J = 2.5 Hz, 1H), 7.40–7.43 (m, 3H), 7.53 (s, 1H), 7.75 (d, J = 8.8 Hz, 1H), 12.33 (br s, 1H, dis. with D_2O). Anal. ($C_{19}H_{15}ClO_5$) C, H.

7.1.8. 3-{7-[(3-Chlorobenzyl)oxy]-2-oxo-2H-chromen-4-yl} propanamide (**76**)

Carboxylic acid derivative **75** (0.25 g, 0.69 mmol) was suspended in dry dichloromethane (5 mL) and thionyl chloride (5 mL) was added. After refluxing for 2 h, the solvent and the excess $SOCl_2$ were removed under rotary evaporation and aq. ammonia (10 mL) was slowly added to the oil residue, while cooling at 0 °C. The reaction mixture was kept under magnetic stirring at room temperature overnight. The resulting precipitate was filtered and washed with water, furnishing the crude product that was crystallized from hot ethanol and then recrystallized from hot methanol. Yield: 94%. Mp: 183–4 °C. ^{1}H NMR (300 MHz, DMSO-d_6) δ: 2.43 (t, J = 7.1 Hz, 2H), 2.97 (t, J = 7.1 Hz, 2H), 5.23 (s, 2H), 6.12 (s, 1H), 6.90 (br s, 1H, dis. with D_2O), 7.04 (dd, J_1 = 2.5 Hz, J_2 = 8.8 Hz, 1H), 7.08 (d, J = 2.5 Hz, 1H), 7.40–7.44 (m, 4H, 1H dis. with D_2O), 7.54 (s, 1H), 7.75 (d, J = 8.8 Hz, 1H). Anal. ($C_{19}H_{16}ClNO_4$) C, H, N.

7.1.9. 3-{7-[(3-Chlorobenzyl)oxy]-2-oxo-2H-chromen-4-yl} propanenitrile (**77**)

Amide **76** (0.11 g, 0.30 mmol) was suspended in dry dioxane (3 mL) and pyridine (0.49 μL, 0.60 mmol) was added, followed by trifluoroacetic anhydride (0.15 mL, 1.1 mmol) at 0 °C through an external ice-bath. The mixture was slowly warmed at ambient temperature and then stirred for 1 h, before pouring onto crushed ice (~30 g). The aqueous phase was extracted with chloroform (3 × 30 mL) and the organic layers were collected, dried over Na_2SO_4 and concentrated under reduced pressure giving a crude product that was purified through flash chromatography (gradient eluant: methanol in dichloromethane 0%→5%). The white solid isolated was crystallized from hot ethyl acetate, thus furnishing the desired product. Yield: 86%. Mp: 138–140 °C. ^{1}H NMR (300 MHz, DMSO-d_6) δ: 2.92 (t, J = 7.1 Hz, 2H), 3.12 (t, J = 7.1 Hz, 2H), 5.24 (s, 2H), 6.28 (s, 1H), 7.04 (dd, J_1 = 2.5 Hz, J_2 = 8.8 Hz, 1H), 7.10 (d, J = 2.5 Hz, 1H), 7.40–7.43 (m, 3H), 7.53 (s, 1H), 7.78 (d, J = 8.8 Hz, 1H). Anal. ($C_{19}H_{14}ClNO_3$) C, H, N.

7.1.10. N^2-{7-[(3-Chlorobenzyl)oxy]-2-oxo-2H-chromen-4-yl} glycinamide (**78**)

To a suspension of glycinamide hydrochloride (0.20 g, 1.8 mmol) in dry DMF (6.0 mL), DIEA (0.62 mL, 3.6 mmol) was added and the mixture was stirred for 15 min at room temperature. 4-Chloro-7-[(3-chlorobenzyl)oxy]-2*H*-chromen-2-one **5** [21] (0.19 g, 0.60 mmol) was added and the mixture was heated at 90 °C for 4 h. After evaporation of the solvent under reduced pressure, the oil residue was purified through column chromatography (eluant: methanol in dichloromethane 5% v/v). Yield: 89%. Mp: 216 °C (dec.). ^{1}H NMR (300 MHz, DMSO-d_6) δ: 3.79 (d, J = 6.1 Hz, 2H), 4.83 (s, 1H), 5.21 (s, 2H), 6.96 (d, J = 2.5 Hz, 1H), 7.01 (dd, J_1 = 2.5 Hz, J_2 = 8.8 Hz, 1H), 7.20 (br s, 1H, dis. with D_2O), 7.40–7.43 (m, 3H), 7.53 (s, 1H), 7.56 (br s, 1H, dis. with D_2O), 7.88 (t, J = 6.1 Hz, 1H, dis. with D_2O), 7.91 (d, J = 8.8 Hz, 1H). Anal. ($C_{18}H_{15}ClN_2O_4$) C, H, N.

7.1.11. N-[7-(3-chlorobenzyloxy)-2H-2-oxochromen-4-yl]-2-chloroacetamide (**79**)

4-Amino-7-[(3-chlorobenzyl)oxy]-2*H*-chromen-2-one **12** [21] (0.18 g, 0.60 mmol), chloroacetyl chloride (0.048 mL, 0.60 mmol) and DIEA (0.11 mL, 0.60 mmol) were refluxed under magnetic stirring in anhydrous THF (3 mL) for 48 h. After filtration and evaporation of the solvent, the residue was crystallized from ethanol. Yield: 49%. ^{1}H NMR (DMSO-d_6) δ: 4.50 (s, 2H), 5.23 (s, 2H), 6.98–7.08 (m, 3H), 7.35–7.46 (m, 3H), 7.50 (s, 1H), 7.79 (d, J = 9.6 Hz, 1H), 10.28 (br s, 1H, dis. with D_2O). Anal. ($C_{18}H_{13}Cl_2NO_4$) C, H, N.

7.2. Biological assays

MAO inhibitory activity of compounds in Tables 1–2 was assessed using a continuous spectrophotometric assay, monitoring the rate of oxidation of the nonselective nonfluorescent MAO substrate kynuramine to 4-hydroxyquinoline. Briefly, male Sprague–Dawley rats (200–250 g) were sacrificed by decapitation. The brains were immediately removed and washed in an ice-cold isotonic Na_2HPO_4/KH_2PO_4 buffer (pH 7.40) containing sucrose. A crude brain mitochondrial fraction was then prepared by differential centrifugation [34] and stored at −40 °C in an isotonic Na_2HPO_4/KH_2PO_4 buffer (pH 7.4) containing KCl. MAO-A and MAO-B activities were assayed after pre-treatment of mitochondrial preparations (1 mg/mL) with the selective and irreversible inhibitors (−)-L-deprenyl (250 nM) and clorgyline (250 nM), respectively. After a preincubation for 5 min with the assayed compound dissolved in DMSO at a final concentration of 5% (v/v), kynuramine was added at a concentration equal to the corresponding K_M value (90 μM for MAO-A and 60 μM for MAO-B). Then

the rate of formation of 4-hydroxyquinoline was monitored at 314 nm for 5 min. Finally, IC_{50} values were determined by nonlinear regression of MAO inhibition vs. −log of the concentration plots, using the program Origin, version 6.0 (Microcal Software Inc., Northampton, MA).

7.3. Computational methods

The coumarin inhibitors were built from the LigPrep module available in Maestro (vers. 9.2) starting from the reference ligand that is the 4-formyl-7-*m*-chlorobenzyloxycoumarin (4-FCBC) co-crystallized with humanMAO-B (PDB code: 2v60) [35]. As already reported [20], the spatial model of the ratMAO-B was constructed through homology modeling. According to a recent study of humanMAO-B crystal structure, we designated eight water molecules as ordered and labeled them as w1055, w1159, w1166, w1171, w1206, w1224, w1309 and w1351 referring to the numbering of the X-ray structure of humanMAO-B in complex with 4-FCBC.

7.3.1. Docking simulations

GOLD (vers. 5.2), a genetic algorithm-based software, was used for the docking study selecting GoldScore as a fitness function. GoldScore is made up of four components that account for protein-ligand binding energy: protein-ligand HB energy (external HB), protein-ligand van der Waals energy (external vdw), ligand internal vdw energy (internal vdw), and ligand torsional strain energy (internal torsion). Parameters used in the fitness function (HB energies, atom radii and polarizabilities, torsion potentials, HB directionalities, and so forth) were taken from the GOLD parameter file. For each coumarin inhibitor, 10 conformations were generated in a sphere of a 12 Å radius centered on the phenolic oxygen atom of Y435. In our docking runs, the molecular scaffold of the best ranked solution of the reference ligand (PDB code: 2v60) docked into the ratMAO-B was set as physical constraint to favor the occurrence of the known binding mode of *m*-halogeno-7-benzyloxy substituents of coumarin inhibitors (together with a distance constraint between the backbone oxygen atom of I164 and halogen atom of the inhibitor). Docking simulations towards MAO-B were carried out by allowing torsions and flexibility to Q206.

7.3.2. 3D-QSAR

Inhibitor molecules were built using as a structural reference the 4-FCBC co-crystallized with humanMAO-B (PDB code: 2v60). The substituent at position 4 of 4-FCBC was properly replaced by using the organic fragment library available from Schrodinger. LigPrep [36] was used to check the occurrence of tautomeric, stereochemical, and ionization variations, as well as for preliminary energy minimization. The modeled structures were, thus, docked into the MAO-B binding site to enable the sampling of the allowed conformational space at position 4. The obtained top-scored docking poses were, thus, superimposed by limiting the manual intervention to maximize, whenever it was necessary, the structural match of the common coumarin scaffold. Subsequently, the Gaussian steric, electrostatic, hydrophobic, HBA and HBD interaction energies were calculated at 1.0 Å regularly spaced grid whose size comprised a molecular region beyond 3.0 Å the training set limits [37]. In particular, a dummy probe was used to calculate the steric [38] and hydrophobic [39] field; a +1 point charge probe [38] to measure the electrostatic field; an acceptor/donor probe [40] for the HBA and HBD field. Force fields terms within 2.0 Å of any training set atom were ignored whereas steric and electrostatic terms were truncated at 30.0 kcal/mol. Variables having $|t\text{-value}| < 2.0$ were eliminated.

References

[1] M.B.H. Youdim, J.P.M. Finberg, K.F. Tipton, in: U. Trendelenburg, N. Weiner (Eds.), Catecholamine II. Handbook of Experimental Pharmacology, Springer, Berlin, 1988, pp. 127–199.
[2] J.P. Johnston, Biochem. Pharmacol. 17 (1968) 1285–1297.
[3] A.S. Kalgutkar, D.K. Dalvie, N. Castagnoli Jr., T.J. Taylor, Chem. Res. Toxicol. 14 (2001) 1139–1162.
[4] J. Grimsby, N.C. Lan, R. Neve, K. Chen, J.C. Shih, J. Neurochem. 55 (1990) 1166–1169.
[5] C. Binda, M. Li, F. Hubalek, N. Restelli, D.E. Edmondson, A. Mattevi, Proc. Natl. Acad. Sci. U. S. A. 100 (2003) 9750–9755.
[6] L. De Colibus, M. Li, C. Binda, A. Lustig, D.E. Edmondson, A. Mattevi, Proc. Natl. Acad. Sci. U. S. A. 102 (2005) 12684–12689.
[7] D.E. Edmondson, A. Mattevi, C. Binda, M. Li, F. Hubálek, Curr. Med. Chem. 11 (2004) 1983–1993.
[8] M.B. Youdim, D.E. Edmondson, K.F. Tipton, Nat. Rev. Neurosci. 7 (2006) 295–309.
[9] M. Naoi, W. Maruyama, Curr. Pharm. Des. 16 (2010) 2799–2817.
[10] M. Wimbiscus, O. Kostenko, D. Malone, Clev. Clin. J. Med. 77 (2010) 859–882.
[11] M. Bortolato, K. Chen, J.C. Shih, Adv. Drug Deliv. Rev. 60 (2008) 1527–1533.
[12] G. Cohen, R. Farooqui, N. Kesler, Proc. Natl. Acad. Sci. U. S. A. 94 (1997) 4890–4894.
[13] M. Carmo Carreiras, E. Mendes, M. Jesus Perry, A.P. Francisco, J. Marco-Contelles, Curr. Top. Med. Chem. 13 (2013) 1745–1770.
[14] M.T. Lin, M.F. Beal, Nature 443 (2006) 787–795.
[15] L. Pisani, M. Catto, F. Leonetti, O. Nicolotti, A. Stefanachi, F. Campagna, A. Carotti, Curr. Med. Chem. 18 (2011) 4568–4587.
[16] J. Saura, J.M. Luque, A.M. Cesura, M. Da Prada, V. Chan-Palay, G. Huber, J. Loffler, J.G. Richards, Neuroscience 62 (1994) 15–30.
[17] F. Leonetti, C. Capaldi, L. Pisani, O. Nicolotti, G. Muncipinto, A. Stefanachi, S. Cellamare, C. Caccia, A. Carotti, J. Med. Chem. 50 (2007) 4909–4916.
[18] C. Brühlmann, F. Ooms, P.A. Carrupt, B. Testa, M. Catto, F. Leonetti, C. Altomare, A. Carotti, J. Med. Chem. 44 (2001) 3195–3198.
[19] A. Carotti, MAOs long March: from toxic first-generation drugs to isoform-selective, reversible and multi-target inhibitors, in: Proceedings of ACS-EFMC Meeting Frontiers in CNS and Oncology Medicinal Chemistry, Siena, Italy, October 7-9, 2007.
[20] L. Pisani, G. Muncipinto, T.F. Miscioscia, O. Nicolotti, F. Leonetti, M. Catto, C. Caccia, P. Salvati, R. Soto-Otero, E. Mendez-Alvarez, C. Passeleu, A. Carotti, J. Med. Chem. 52 (2009) 6685–6706.
[21] L. Pisani, M. Catto, O. Nicolotti, G. Grossi, M. Di Braccio, R. Soto-Otero, E. Mendez-Alvarez, A. Stefanachi, D. Gadaleta, A. Carotti, Eur. J. Med. Chem. 70 (2013) 723–739.
[22] A. Carotti, C. Altomare, M. Catto, C. Gnerre, L. Summo, A. De Marco, S. Rose, P. Jenner, B. Testa, Chem. Biodivers. 3 (2006) 134–149.
[23] M. Catto, O. Nicolotti, F. Leonetti, A. Carotti, A.D. Favia, R. Soto-Otero, E. Mendez-Alvarez, A. Carotti, J. Med. Chem. 49 (2006) 4912–4925.
[24] M.L. Verdonk, J.C. Cole, M.J. Hartshorn, C.W. Murray, R.D. Taylor, Proteins 52 (2003) 609–623.
[25] O. Nicolotti, I. Giangreco, T.F. Miscioscia, A. Carotti, J. Chem. Inf. Model 49 (2009) 2290–2302.
[26] S.L. Dixon, A.M. Smondyrev, E.H. Knoll, S.N. Rao, D.E. Shaw, R.A. Friesner, J. Comput. Aided Mol. Des. 20 (2006) 647–671.
[27] Phase, Version 3.1, Schrödinger, LLC, New York, NY, 2009.
[28] S. Güssregen, H. Matter, G. Hessler, M. Müller, F. Schmidt, T. Clark, J. Chem. Inf. Model 52 (2012) 2441–2453.
[29] L. Pisani, M. Barletta, R. Soto-Otero, O. Nicolotti, E. Mendez-Alvarez, M. Catto, A. Introcaso, A. Stefanachi, S. Cellamare, C. Altomare, A. Carotti, J. Med. Chem. 56 (2013) 2651–2664.
[30] F. Campagna, A. Carotti, G. Casini, Tetrahedron Lett. 21 (1977) 1813–1816.
[31] E. Mendez-Alvarez, R. Soto-Otero, I. Sanchez-Sellero, L.M. Lopez-Rivadulla, M. Lamas, Life Sci. 60 (1997) 1719–1727.
[32] A. Gissi, D. Gadaleta, M. Floris, S. Olla, A. Carotti, E. Novellino, E. Benfenati, O. Nicolotti, Altex 31 (2014) 23–36.
[33] C.M. Sousa, J. Berthet, S. Delbaere, P.J. Coelho, J. Org. Chem. 77 (2012) 3959–3968.
[34] R. Soto-Otero, E. Mendez-Alvarez, A. Hermida-Ameijeiras, I. Sanchez-Sellero, A. Cruz-Landeira, M.L.R. Lamas, Life Sci. 69 (2001) 879–889.
[35] C. Binda, J. Wang, L. Pisani, C. Caccia, A. Carotti, P. Salvati, D.E. Edmondson, M. Mattevi, J. Med. Chem. 50 (2007) 5848–5852.
[36] LigPrep, Version 2.3, Schrödinger, LLC, New York, NY, 2009.
[37] R.C. Wade, in: G. Cruciani (Ed.), Molecular Interaction Fields. Applications in Drug Discovery and ADME Prediction, Wiley-VCH, Weinheim, 2005, pp. 27–42.
[38] J.L. Banks, H.S. Beard, Y. Cao, A.E. Cho, W. Damm, R. Farid, A.K. Felts, T.A. Halgren, D.T. Mainz, J.R. Maple, R. Murphy, D.M. Philipp, M.P. Repasky, L.Y. Zhang, B.J. Berne, R.A. Friesner, E. Gallicchio, R.M. Levy, J. Comp. Chem. 26 (2005) 1752–1780.
[39] A.K. Ghose, N. Vellarkad, N.V. Viswanadhan, J.J. Wendoloski, J. Phys. Chem. A 102 (1998) 3762–3772.
[40] M. Böhm, G. Klebe, J. Med. Chem. 45 (2002) 1585–1597.